Fast 3-D Inductance Extraction in Lossy Multi-Layer Substrate

Minqing Liu
Computer Engineering
University of California, Santa Cruz
Santa Cruz,CA 95064
liumq@cse.ucsc.edu

Tiejun Yu
Cadence Design Systems
555 River Oaks Parkway
San Jose, CA95134
tiejun@cadence.com

Wayne W.-M. Dai
Computer Engineering
University of California, Santa Cruz
Santa Cruz, CA 95064
dai@cse.ucsc.edu

Abstract

A mixed potential integral equation (MPIE) technique combined with fast multi-layer Green's functions and Gaussian Jacobi high order techniques is used to compute the 3-D frequency dependent inductances and resistances in lossy multi-layered substrate. Compared to FastHenry, a multipole-accelerated 3-D inductance extraction program, the algorithm presented here is more accurate and faster for lossy multilayer structures due to two reasons. First, substrate and optional ground plane's lose and coupling effect are efficiently modeled by multilayer Green's functions, while the Green's functions are efficiently calculated via window-based acceleration technique. Second, Gaussian Jacobi-based high order techniques are used to capture the singularity of the current distribution at metal edges, leading to significant reduction of problem size and speed-up of computation.

1 Introduction

Radio frequency (RF) circuits fabricated in monolithic microwave integrated circuit technologies (such as CMOS MMIC) make extensive use of on-chip transmission lines to realize an inductance. Inductors are usually implemented as spiral structures. The spiral inductor is a key component in many high-performance and narrow-band circuit designs. Fabrication of spiral inductors on the same substrate as the rest of RF circuit can obviate the external connections, electrical and magnetic coupling, pad and bond wire parasitic. In order to exploit capabilities offered by a monolithic inductance, the limits imposed by silicon technology, primely the substrate lossy, must be accurately modeled and characterized. Despite extensive recent work [8, 2, 1, 3, 4], there are still many rooms for improvement, especially on lossy substrate coupling.

FastHenry, based on the magnetoquasistatic assumption, is one of the most popular techniques to extract inductance [8]. It uses fast multipole method (FMM) [8] to accelerate matrix-vector production. With the Generalized Minimal Residual (GMRES) matrix solution algorithm, FastHenry achieves nearly linear time and space with respect to the number of volume-filaments. However, using FastHenry to do parameter extraction for lossy layered spiral inductors, we have to discretize not only the spiral metal wire, but also the heavily doped substrate and ground plane. For a typical spiral inductor on-chip, more than 90% volume filaments have to be used to discretize the substrate and ground plane, which leads to huge unknown size and extremely ex-

pensive computation even with FMM. In this paper, we use multilayer Green's functions to take care of the layered media, the substrate loss and the ground plane, and only discretize spiral metal. This results in a full wave integration equation and significant reduction of the unknown size, but it also involves a time-consuming calculation of multilayer Green's function which comprises Sommerfeld-type integrals. Fortunately, [13, 5] developed a window-based accelerating technique, and significantly speeds up the Green's function computation. This fast Green's function technique is used here.

With discretization on spiral metal wires, the unknown size may be still very large due to the fact that the current distribution on spiral metal wires varies dramatically in the transverse direction because of the skin, proximity and edge effects. To further reduce the unknown size, the advanced high order technique is also used in this paper. High order technique means using coarser discretization and bigger support of basis function, but traditional high order techniques are limited by using smooth basis functions to deal with the singularity problem [18]. The high order Gaussian quadrature we use here can capture the practical singularity features and further reduce the number of unknowns.

The RWG basis function based on method of moment (MoM) is a standard technique used in the perfect electrical conducting (PEC) surface IE [6]. For non-PEC cases, surface impedance can be introduced when the boundary condition is used at the metal surface to establish the integral equation. However, as the metal thickness is at the order of the skin depth, which is just the case in the RF spiral inductance on-chip, it is not easy to define the metal surface impedance. So, we use volume roof-top basis function on the rectangular bar pairs instead of surface RWG basis function. Similar to the rectangular filament used in FastHenry, this new volume basis function can easily handle the metal loss. At the same time, this new basis function keeps the roof-top feature of the RWG basis function which offers the current continuous to the neighbor filaments, and hence, no fictitious charge singularities arise. Another benefit from the basis functions is that it easily incorporates with high order Gaussian-Jacobi Quadratures (GJQ).

With the techniques described above, the problem size is reduced to a few hundreds for a typical spiral inductor on chip, and FMM is unnecessary. LU decomposion (LUD) is used for final matrix inversion.

In section II, we start with the problem set up by establishing the integral equation. Then in Section III we introduce the Fast Green's function. In section IV, the GJQ high order technique is summarized. Finally we provide the numerical experiments and draw our conclusion in section V and VI respectively.

2 Integral Equation

Combining MPIE and the relationship $\mathbf{J} = \sigma\mathbf{E}$, we easily arrive the following equation [19]:

$$\mathbf{E^i} = \frac{\mathbf{J}}{\sigma} - \frac{j\omega\mu_0}{4\pi} \int_{v'} G_A(r, r') \cdot \mathbf{J}(r') dV'$$
$$- \frac{j}{4\pi\omega\varepsilon_0} \nabla \int_{v'} G_V(r, r') \nabla' \cdot \mathbf{J}(r') dV' \tag{1}$$

where G_A and G_V are the vector and scalar potential multilayer Green functions respectively; G_A is a dyadic with 9 terms. While via's effects are usually ignored and without vertical current in the problem, G_A here is also reduced to a scalar number which in fact is $G_A{}^{xx}$. $\mathbf{J}(r')$ is the current distribution in the conductor embedded in the multilayer media; $\mathbf{E}^i$ is the incident electric field added at the ends of the metal ports. Compared to the integral equation used in FastHenry, Green's function is used here instead of 1/r used in FastHenry. In this way, we do not need to discretize the substrate and ground plane. To properly capture skin and proximity effects in those conductors, the cross section of them is divided into a bundle of parallel filaments as shown in Figure 1. However with the high order technique described in section IV, the division number of this transverse discretization is very low. Once the conductors are discretized into filaments, the interconnection of current filaments can be represented as Figure 1. The current in the conductor can be approximated as:

$$\mathbf{J}(r) \approx \sum_{i=1}^{N} I_i \mathbf{f_i(r)} \tag{2}$$

where N is the number of nodes which are associated with connection points between filaments. The basis function $\mathbf{f_i}$ is defined as:

$$\mathbf{f}_i(r) = \begin{cases} \frac{\mathbf{l}_i^+(r)}{V_i^+}, & \text{r in } V_i^+ \\ \frac{\mathbf{l}_i^-(r)}{V_i^-}, & \text{r in } V_i^- \\ 0, & \text{otherwise} \end{cases} \tag{3}$$

where $\mathbf{l}_i(r)$ is a vector along the length of the ith filament as shown in Figure 2, V_i the volume of the filament i, and I_i the current flowing through the ith node. If we assume the nodes of the two ends of a filament are I_i^+ and I_i^-, we can obtain:

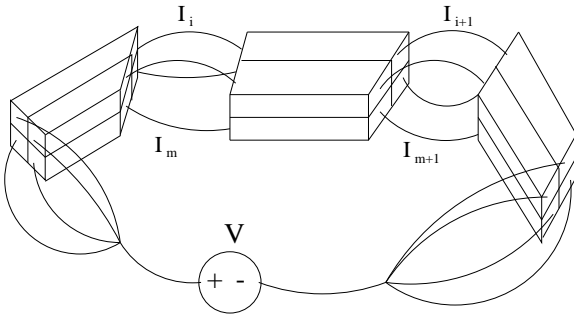$$\nabla \cdot \mathbf{J}(\mathbf{r}) = \frac{I_i^+ - I_i^-}{2V_i} \tag{4}$$

Figure 1: *Conductor divided as filaments*

Applying the MoM process in a system with n terminal nodes, we reach the following system equation:

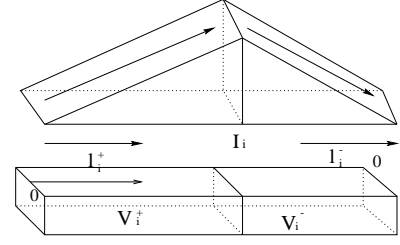$$[Z_{ij}]_{N \times N}[I_j]_{N \times 1} = [V_j]_{N \times 1} \tag{5}$$

Figure 2: *One geometry for the construction of a vector volume basis function $\mathbf{f}_i(r)$, $\mathbf{l}_i^\pm(r)$ is a position vector in the volume $V_i^\pm$*

where I_j is the unknown we want to calculate, $V_j = < \mathbf{E}^i, \mathbf{f}_j(r) >$ is the terminal exciting and Z_{ij} is a frequency dependent impedance matrix whose elements are represented as:

$$Z_{ij}(\omega) = R_{ij} + j\omega L_{ij} + K_{ij}/(j\omega) \tag{6}$$

where

$$R_{ij} = \begin{cases} \frac{1}{2\sigma}(\frac{l_i^+}{S_i^+} + \frac{l_i^-}{S_i^-}) & i = j \\ 0 & i \neq j \end{cases} \tag{7}$$

$$L_{ij} = L'_{i^+ j^+} + L'_{i^- j^+} + L'_{i^+ j^-} + L'_{i^- j^-} \tag{8}$$
$$K_{ij} = K'_{i^+ j^+} - K'_{i^- j^+} - K'_{i^+ j^-} + K'_{i^- j^-} \tag{9}$$

where i, j are the sequence numbers of the nodes connected filaments. i^+, i^- are the sequence numbers of the filaments at the two sides of node i, and j^+, j^- are the sequence numbers of the filaments at the two sides of node j. R', K', and L' are given by

$$R'_{nn} = \frac{l_n}{2\sigma S_n} \tag{10}$$

$$L'_{mn} = \int_{v_m} \int_{v_n} G_A(r_m, r_n) \mathbf{f}_m(r) \mathbf{f}_n(r) dv\, dv \tag{11}$$

$$K'_{mn} = \frac{1}{v_m v_n} \int_{v_m} \int_{v_n} G_V(r_m, r_n)\, dv\, dv \tag{12}$$

where $m, n = i^\pm, j^\pm$ are the sequence numbers of the filaments, and l_n is the length of the filament n. By solving the matrix equation (5), we can extract the current distribution in the conductors and then deduce other parameters, such as S, Y parameters, and Q factor. But there are two bottlenecks in solving equation (5): one is filling the impedance matrix Z_{ij} which involves the Green's function calculation; the other is solving the matrix which is $O(n^3)$ if LU decomposition is used. The following two sections will give the solutions for these two problems.

3   Fast Green's Function

Green's function and integral equations, which arise in layered media problems, comprise Sommerfeld-type integrals of the following form

$$G(\rho) = S_n\left[\widetilde{G}(k_\rho)\right] = \int_0^\infty \widetilde{G}(k_\rho) J_n(k_\rho\rho) k_\rho^{n+1} dk_\rho \tag{13}$$

where G is the Green's function we need, and $\widetilde{G}$ is the Green's function in the spectral domain which can be obtained by a transmission line technique [11].

The above integral contains a Bessel function J_n which oscillates very fast (especially when the transverse distance ρ between the source and observation points is large) and decays slowly. In addition, $\widetilde{G}$ does not behave well, especially when the number of layers is large. There

are many papers on fast calculation of Green's function of multilayered structures [10, 9]. Most of them use complex image method (CIM) based on the Prony method and the well-known Sommerfeld identity. CIM is a powerful tool to calculate the Green's function when the source and field points remain in the same layer and the frequency belongs to some proper domain. However, in some cases, CIM seems not to work very well because of the difficulty of pole extraction and other difficulties such as different layer problems. In [7], an efficient evaluation of Green's function which is based on the integration on the steepest-descent paths (SDP) was proposed. However, it is only valid for simple structures, e.g. the case of half space, in which SDP can really be found out. [13] proposed and developed a robust and general method of fast Green's function calculation for multilayered structures which is an application of the window functions derived in [5]. We summarize this new technique here for completeness. The idea is to use a low pass filter (LPF) window function to create the artificial SDP so that the integral length is greatly reduced in equation (13). Using the following identity for the cylindrical symmetrical Green's function $G(\rho)$, we can get:

$$G(x,y) * \psi(x,y) = S_0 \left[\widetilde{G}(k_\rho) \, \widetilde{\psi}(k_\rho) \right] (\rho) \tag{14}$$

where S_0 is the first order Sommerfeld integral defined in (13), $\widetilde{\psi}$ is the special LPF window function given in [13, 5]. Compared to (13), the integral kernel in (14) decays much faster due to the fast decaying factor $\widetilde{\psi}$, so the integral length will be greatly reduced. However, what we get now is the convolution of $G(x,y)$ with $\psi(x,y)$, instead of only $G(x,y)$. To recover the value of $G(x,y)$ from the left-side of equation (14), we use the Taylor expansion method to expand function $G(x,y)$ at point (x,y), then we obtain:

$$G(x,y) * \psi(x,y) \approx M_0 G(x,y) + M_2 (G_{xx}(\xi,0) + G_{yy}(\xi,0)) \tag{15}$$

where $0 \leq \xi \leq \rho = \sqrt{x^2 + y^2}$, and the zero order moment is

$$M_0 = \int_{\sqrt{x^2+y^2} \leq a} \psi(x,y) dx dy = \frac{\pi a^2}{m+1} \tag{16}$$

Where a is the support of the window function [5]. The first moment $M_1 = 0$, and the second one $M_2 \to 0$. As a result of (14) and (15), the fast Green's function algorithm can be approximately expressed as:

$$G(\rho) = \frac{1}{M_0} S_0 \left[\widetilde{G}(k_\rho) \, \widetilde{\psi}(k_\rho) \right] (\rho) + O(a^2), \quad when \ \ a \to 0. \tag{17}$$

With the above techniques, Green's functions are easily obtained and the database of the 3-D Green's function can be established quickly. When matrix Z in equation (6) is filled, the database of the Green's function is used to interpolate the $G(\rho)$ we need. For one typical technique profile, the database can be used repeatedly and save the CPU time significantly.

4 High Order Technique

Compared to FMM [8] and singularity value decomposition (SVD) [15], reducing the problem size is the most efficient and direct way to reduce inversion time of matrix. In addition, FMM has its own limits. It is an integral kernel dependent technique, which means the $1/r$ or e^{-jkr}/r form of the Green's function must be used. A high order technique is an efficient way to reduce the problem size. With the understanding of the edge current singularity on a metal strip line, a high order Gaussian-Jacobi quadrature (GJQ) technique [12] is used to capture the current distribution characteristic in the transverse direction of the long thin metals, which leads to less discretization along the transverse direction and thus greatly reduces the total problem size.

4.1 Extraction of Current Singularity

An integral equation based on MoM usually leads to a density matrix inversion. Due to the existing singularity of current at the edges and the corners of conductors, the metal must be discretized into enough fine subdomains at the edges and the corners to represent the actual situation in a traditional MoM process, thus the matrix obtained from classical MoM is usually large even for a simple problem like on-chip spiral inductors. It is well known that, for an infinite thin metal strip, the transverse current distribution at the metal edge behaves in a singularity form of $r^{-1/2}$ [16, 17], where r is the distance to the edge. Understanding the edge singularity features of a long thin metal strip, and placing the original point of the abscissa in the middle of the cross section of the conductor shown in Figure 3, we can reasonably present the transmission current distribution as:

$$\mathbf{J}_z(r) = s(x,y)\mathbf{f}_z(r) \tag{18}$$

where

$$s(x,y) = \frac{1}{(1-(\frac{2x}{W})^2)^{1/2}(1-(\frac{2y}{h})^2)^{1/2}} \tag{19}$$

and

$$\nabla \cdot \mathbf{J}_z(r) = s(x,y) \nabla \cdot \mathbf{f}_z(r) \tag{20}$$

In this way, the singularity part of the current distribution $s(x,y)$ is extracted out. Here the singularity order of s is -1/2. We only need to solve the smooth part $\mathbf{f}_z(r)$, instead of $\mathbf{J}_z(r)$. The problem now is how to extract the singularity part of the current $s(x,y)$ when doing integral in MoM. the Gaussian-Jacobi Quadrature (GJQ) rule is just what exactly meets the needs. Before we talk about GJQ, one thing which needs to be made clear is that the practical singularity order of a thickness metal at the edge is actually less than the order of the above $s(x,y)$, This does not matter when we use the above extraction, because the redundant singularity will be concealed by $\mathbf{f}_z(r)$.
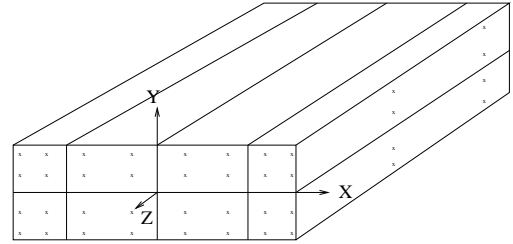

Figure 3: *Gauss-Jacobi discretization in a section of a conductor*

4.2 Gaussian-Jacobi Quadrature (GJQ)

The definite integral of a relative smooth function $f(x)$ can be approximated through the quadrature formula:

$$\int_a^b f(x)dx \approx \sum_{k=1}^n B_k f(x_k) \tag{21}$$

For a singularity function $w(x)f(x)$, $w(x)$ is the singularity part like $s(x)$ defined above, and $f(x)$ is the smooth part. The definite integral of $w(x)f(x)$ can also be approximately expressed via the GJQ formula:

$$\int_a^b w(x)f(x)dx \approx \sum_{k=1}^n A_k f(x_k) \tag{22}$$

where x_k are quadrature points and A_k are called weights. The difference between the above two schemes is that GJQ can handle singularity

integral kernel while the other can only be used for smooth integral kernel. With a given order n and an exact weight singularity function $w(x)$, the n points abscissa $x_k(k=1,\ldots,n)$ and weights $A_k(k=1,\ldots,n)$ can be determined uniquely in GJQ schemes[12]. With the weight function $w(x) = (1-x)^\alpha \cdot (1+x)^\beta$, known as Jacobi polynomials, GJQ can give $2n-1$ degrees of polynomial precision. GJQ is useful to extract the singularity of current distribution in the integral equation. Applying the equation (18) and (20) to the equation (1), we can rewrite the integral equation as:

$$\mathbf{E^i} = \frac{\mathbf{J}}{\sigma} - \frac{j\omega\mu_0}{4\pi}\int_{s'} s(r')G_A(r,r')\mathbf{f}(r')ds'$$
$$-\frac{j}{4\pi\omega\varepsilon_0}\nabla\int_{s'} s(r')G_V(r,r')\nabla'\cdot\mathbf{f}(r')ds'$$

$$(23)$$

where $s(r') = s(x,y)$. Applying GJQ, the above integration becomes:

$$\mathbf{E^i} = \frac{\mathbf{J}}{\sigma} - \frac{-j\omega\mu_0}{4\pi}\sum_{n=1}^{N} A_n \cdot G_A(r,r_n)\cdot\mathbf{f}(r_n)$$
$$-\frac{j}{4\pi\omega\varepsilon_0}\nabla\sum_{n=1}^{N} G_V(r,r_n)\nabla\cdot\mathbf{f}(r_n)$$

$$(24)$$

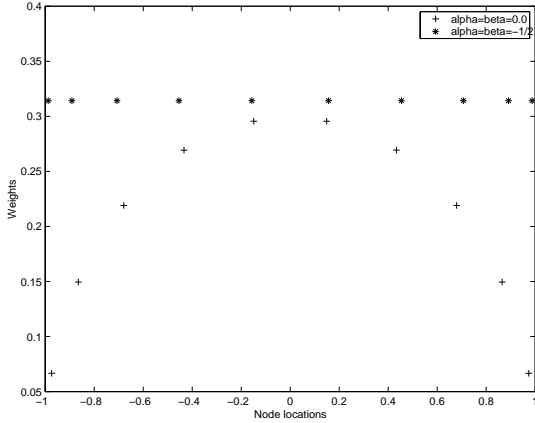where A_n is the weight in the abscissa point r_n.

Figure 4: *Coordinates and weights for typical Gauss-Jacobi polynomials*

Figure 4 depicts the weights and coordinates for two types of Gauss-Jacobi polynomials. $\alpha = \beta = 0$ is used for lengthway discretization which does not have current singularity at the edges. $\alpha = \beta = -1/2$ is used for cross-section discretization. Figure 3 shows the types of Gauss-Jacobi discretization in a section of a conductor. For a high-order scheme, more than one Gauss-Jacobi node is placed in a filament. So R', L', K' in equation (10), (11), (12) can be written down as:

$$R'_{nn} = \frac{A_n}{\sigma}\mathbf{f}_n(r_n)\cdot\hat{l}_n \tag{25}$$

$$L'_{mn} = A_n\mathbf{f}_n(r_n)\int_{v_m} G_A(r,r_n)\mathbf{f}_m(r)\,dv \tag{26}$$

$$K'_{mn} = \frac{A_n}{v_n v_m}\int_{v_m} G_V(r,r_n)dv \tag{27}$$

where r_n is the coordinate of the Gaussian node in filament n, $\mathbf{f}_n(r_n)$ is the value of $\mathbf{f}(r)$ at this Gaussian node, and $\hat{l}_n$ is the unit vector along the length of the nth filament.

layer	high (μm)	ε_r	$\rho\,(\Omega\cdot m)$
diapad	$h=150$	$\varepsilon=1.0$	$\rho=1.78\times10^{-8}$
substarte	$h=420$	$\varepsilon=6.2$	$\rho=1\times10^{10}$
isolate	$h=13$	$\varepsilon=5.0$	$\rho=1\times10^{10}$
dielectric	$h=500$	$\varepsilon=4.5$	$\rho=1.0\times10^{10}$

Table 1: *Parameters (layers are stacked from bottom).*

5 Numerical Experiments

Before we show the GJQ numerical results, we checked the multilayer Green's function. Its accuracy is verified by the direct Sommerfeld integral (DSI). Compared to DSI, it is thousands of times faster. Other successful applications of using the fast multilayer Green's function can be found in [13]. Here is a report from an industry user, who used our tool to design a 5-turn circular spiral inductor on a special CMOS substrate. Table 1 is the technique profile. The spiral inductor and return path embeded on the isolate, and it has the following geometry: number of sides of turn=32, external radius=300μm, metal width=30μm, metal thickness=3.5μm, turn space=6μm. Table 2 presents the results from FastHenry, our simulating tool and the measurement data. The data shows that our tool has improved the loss accuracy compared to FastHenry.

The following numerical experiments focused on showing the effects of the GJQ high order technique.

5.1 Square Spiral Inductors

In practical problems, current distribution at the edge of a conductor demonstrates strong singularity $(1/\sqrt{r})$. Figure 5 shows the "smooth" part at the current distribution in a two-turn square spiral inductor. Figure 6 gives the total current distribution on the inductor. Although the singularities at the edge of a conductor are very strong, by using the GJQ, we can capture the singularity of current efficiently. After we extract the singularities, the remaining parts are very smooth, and easy to be obtained by using less discretization.
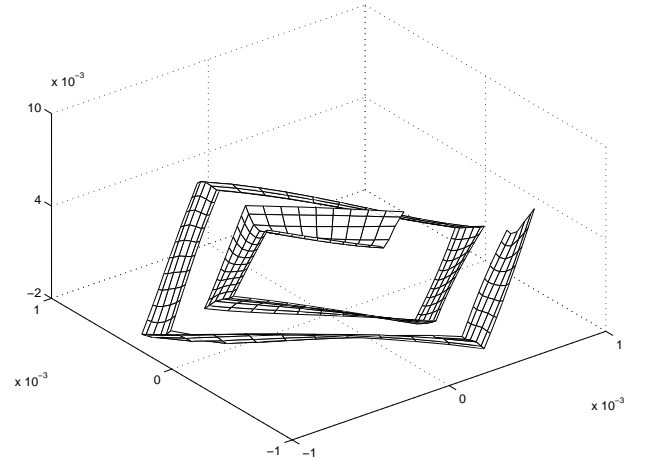

Figure 5: *Smooth part of current distribution $|f_z|$ in a 2-turn inductor at 15GHz*

	FastHenry	Our simulation	Measurements
Rs	3.9(1GHz)	5.0 (at 1GHz), 3.1 (at 3MHz)	3.0 (at 3MHz)
Ls	11.6nH	11.35nH	11.3 nH (at 3 MHz)
Q	17.7	13.57	14 (1GHz)
Q_{max}	32	24	21(3GHz)
F_{max}	–	2.2 GHz	2.0 GHz

Table 2: *Comparison of various parameters for a 5-turn inductor.*
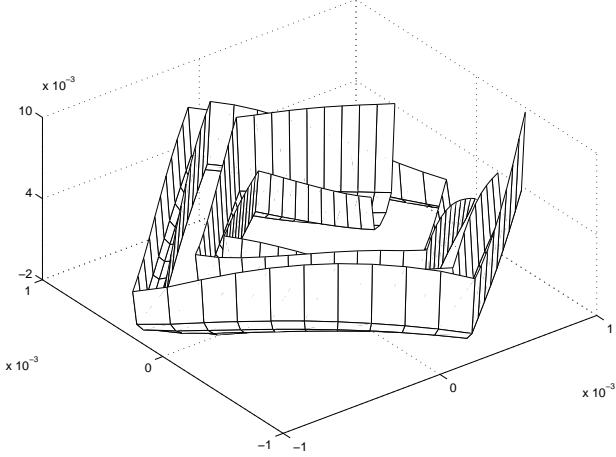
Figure 6: *Total current distribution $|s(x,y) \cdot f_z|$ in a 2-turn inductor at 15GHz*

Figure 7: *Relative error comparison of Gaussian quadrature and uniform discretization schemes*

5.2   Circular Spiral Inductors

Here, we consider an isolated circular spiral inductor presented by a polygon with 12 sides. This is a 4-turn spiral inductor. The metal width and space of the inductor are both $30\mu m$, the radius is $100\mu m$, the metal thickness is $1.27\mu m$, with $\sigma = 3.0 \times 10^7 (\Omega \cdot m)^{-1}$, and the thickness of the silicon substrate is 650μ, with $\rho = 0.5(\Omega \cdot m)$. Table 3 shows the current results at the two ends of the spiral inductor. Since we simulate the inductor by a $1V$ voltage at two ends of it, the current results are the admittance of this spiral inductor. In table 3, the patch number is $48 \times k$, 48 means 12×4, where 4 is the number of turns and each turn has 12 sides. k is the number of cells in the cross section of each side. From table 3, We can find that, for GJQ, when $k = 4$, the relative error is less than 1%, while for the uniform discretization scheme, the number of cells in each segment k must be bigger than 12 for the same accuracy level. Figure 7 shows the convergence performance of the GJQ scheme against the uniform discretization scheme. Compared to the GJQ scheme, the tradition uniform discretization is clearly weak: it is almost impossible to achieve 3-digit accuracy, while the GJQ can achieve 4-digit accuracy only with few Gaussian-quadrature nodes.

6   Conclusion and Future Work

The fast multilayer Green's function and the GJQ high order technique are successfully used to develop a simulation tool for the parameter extraction of spiral inductors on lossy substrates. These techniques capture the substrate loss coupling and the edge current singularity efficiently. Using the multilayer Green's function, only spiral metal needs to be discretized. In some sense, this reduces the problem from 3-D to 2-D. Using GJQ, we turned the unknown, a singularity current distribution $J(r)$, into a smooth function $1/s(x,y) \times J(r)$. This further reduces
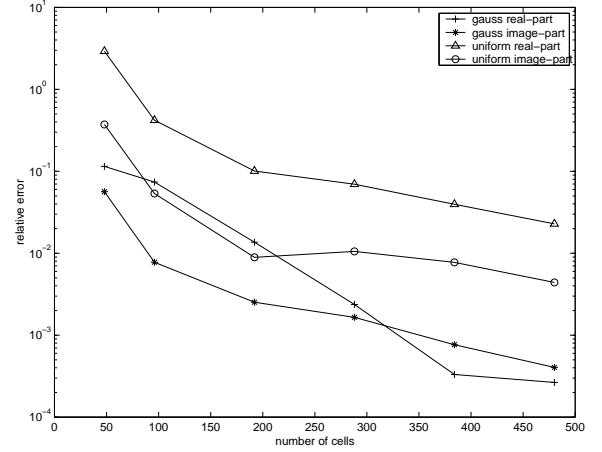
the problem from 2-D to 1-D in some sense. In addition, the GJQ can achieve $2n - 1$ polynomial precision given n nodes along the cross direction. This is because the GJQ nodes and weights are not preassigned but determined by using Hermite interpolation [12]. Apparently, the high frequency skin-effect aggravates the singularity of current. but $1/s(x,y) \times J(r)$ still belongs to smooth parts. In practice, due to the thickness of metal (metal thickness is always greater than zero), the singularity of the current distribution at the edge of metal will become a little smoother than the $s(x,y)$, and this will not affect the precision of the GJQ. Even if $J(r)$ doesn't have the singularity as we regard, when it is multiplied by the $1/s(x,y)$, the difficulty of solving problem is not increased because $1/s(x,y)$ is still a smooth function. With $2n - 1$ polynomial precision, the GJQ schemes can still achieve better accuracy than other high order methods.

Future work includes the use of e^{-jkr}/r based full wave FMM which requires the Green's function solved by an accurate complex image method for lossy layered media. This work is underway in our group and the main problem to be overcome is how to reduce the multipole expansion order when substrate lossy is involved [14]. Another extension of the work is how to efficiently figure out the wideband response of the device from the results of limited frequency points, which are obtained by the above fast algorithms.

7   Acknowledgments

# patchs	uniform scheme	Gauss-Jacobi Quadrature
48×1	1.359900e-02 + j -9.247321e-03	1.629302e-03 + j -1.519477e-02
48×2	3.473050e-03 + j -1.475361e-02	1.841141e-03 + j -1.610331e-02
48×4	2.445925e-03 + j -1.558981e-02	1.987973e-03 + j -1.622929e-02
48×6	2.222174e-03 + j -1.573005e-02	2.015455e-03 + j -1.618842e-02
48×8	2.077681e-03 + j -1.589736e-02	2.020250e-03 + j -1.616177e-02
48×10	1.998564e-03 + j -1.602145e-02	2.019580e-03 + j -1.614940e-02
48×12	2.045273e-03 + j -1.595114e-02	2.019045e-03 + j -1.614286e-02

Table 3: *Comparison of admittance under different discretization.*

REFERENCES

[1] A. M. Niknejad, "Analysis, simulation, and application of passive devices on conductive substrates", *Ph.D. dissertation* , Dept. of ECE, University of California at Berkeley.

[2] J. R. Long, and M. A. Copeland, "The modeling, characterization, and design of the monolithic inductors for silicon RF IC's", *IEEE Journal of solid-state circuits*, vol.32, no.3, pp.357-369, Mar. 1997.

[3] H. M. Greenhouse, "Design of planar rectangular microelectric inductors", *IEEE Trans. on Parts, Hybrids, and Packaging,* vol.10, pp.101-109, June, 1974.

[4] F. W. Grover, *Inductance calculations.* Princeton, NJ: Van Nostrand, 1946.

[5] T. Yu and W. Cai, " High order window functions and fast algorithms for calculating dyadic electromagnetic Green's functions in multilayered media", *Radio Science,* Vol.36, No.4, p.559-570, 2001.

[6] S. M. Rao, D. R. Wilton and A. W. Glisson, "Electromagnetic scattering by surfaces of arbitrary shape", *IEEE Trans. Antennas Propagate*, vol.AP-30, pp. 409-418, 1982.

[7] T. J. Cui and W. C. Chew, "Efficient evaluation of Sommerfeld integrals for TM wave scattering by buried objects," *J. Electromagnetic Wave Appl.,* vol.12, pp.607-657, 1998.

[8] M. Kamon, M. J. Tsuk and J. White, "FastHenry: A multipole accelerated 3-D inductance extraction program", *IEEE Trans.on Microwave Theory and Techniques* vol.42, no.9, pp. 1750-1758, Sept.1994.

[9] M. I. Aksun, "A robust approach for the derivation of closed-form Green's Functions", *IEEE Trans. Microwave Theory Tech.,* vol.44, pp.651-658, May 1996.

[10] Y. L. Chow, J. J. Yang, D. G. Fang and G. E. Howard, "A closed-form spatial Green's Function for the thick microstrip substrate", *IEEE Trans. Microwave Theory Tech.*, vol.39, pp.588-592, Mar. 1991.

[11] K. Michalski and D. Zheng, "Electromagnetic scattering and radiation by surfaces of arbitrary shape in layered media, Part I: Theory" *IEEE Antennas Propagate.*, vol. AP-38, pp. 335-344, Mar.1990.

[12] H. Engels, *Numerical quadrature and cubature*. John Wright and Sons, Ltd., at the Stonebridge Press, Great Britain, 1980.

[13] W. Cai and T. Yu, "Fast calculation of dyadic Green's Function for electromagnetic scattering in the multilayered medium", *Journal of Computational physical. Vol.165, pp.1-21, 2000*

[14] N. Geng, L. Carin, "Fast multipole method for scattering from 3D PEC targets situated in half-space environment", *Micro. Opt. Tech. Lett.,* vol.21, pp. 399-405, June 1999

[15] S. Kapur and J. Zhao, "A fast method of memonts solver for efficient parameter extraction of MCMs", DAC 97, pp.141-146, 1997.

[16] T. Yu and X. Zhang, "The current distribution of high-Tc superconducting microstrip lines", *IEEE Trans. MTT-S Digest,* pp. 1667-1670, 1996.

[17] J. B. Knorr and K. Kuchler, "Analysis of coupled slots and coplanar strips on dielectric substrate", *IEEE Trans. MTT-23*, no.7, pp. 541-548, 1975.

[18] W. Cai, T. Yu and H. Wang, "High-order mixed RWG basis functions for electromagnetic applications", *IEEE Trans. MTT-49*, no.7, pp.1295-1303, 2001.

[19] D.C.Chang and J.X.Zheng, "Electromagnetic Modeling of Passive Circuit Elements in MMIC", *IEEE Trans. MTT-40*, no.9, pp.1741-1747, 1992.